Supporting Information

Highly Sensitive Terbium-Based Metal-Organic Framework Scintillators Applied in Flexible X-ray Imaging

Peng-Kun Wang,[a,b,c] Wen-Fei Wang,[a,b] Bao-Yi Li,[a,b,c] Rui-Xuan Qian,[a,b] Zhao-Xing Gao,[a,b] Shuai-Hua Wang,*[a,b,c] Fa-Kun Zheng*[a,b,c] and Guo-Cong Guo*[a,b,c]

[a] State Key Laboratory of Structural Chemistry, Fujian Institute of Research on the Structure of Matter, Chinese Academy of Sciences, Fuzhou, Fujian 350002, P. R. China

[b] Fujian Science & Technology Innovation Laboratory for Optoelectronic Information of China, Fuzhou, Fujian 350108, P. R. China

[c] University of Chinese Academy of Sciences, Beijing 100049, P. R. China

* Corresponding author to E-mail: shwang@fjirsm.ac.cn; zfk@fjirsm.ac.cn; gcguo@fjirsm.ac.cn

Supplementary figures

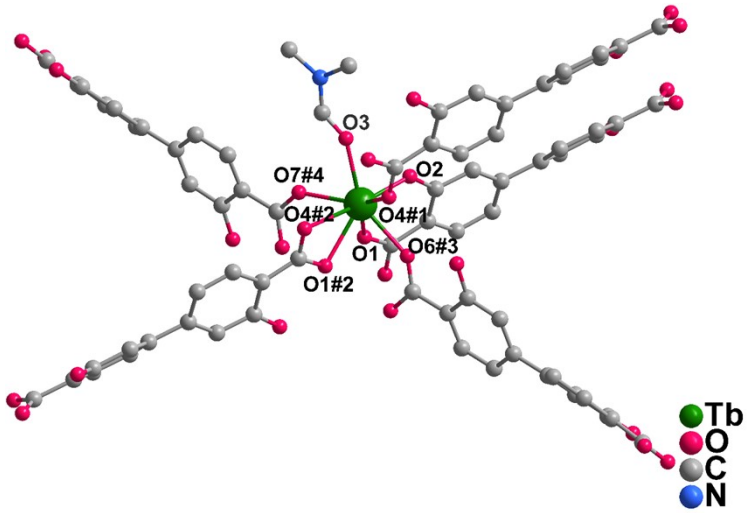

Figure S1 The coordination environment of Tb^{3+}. For clarity, all hydrogen atoms are omitted. Symmetry codes: #1 1 + *x*, *y*, *z*; #2 1 – *x*, –*y*, 1 – *z*; #3 1 – *x*, –1/2 + *y*, 1/2 – *z*; #4 *x*, 1/2 – *y*, 1/2 + *z*.

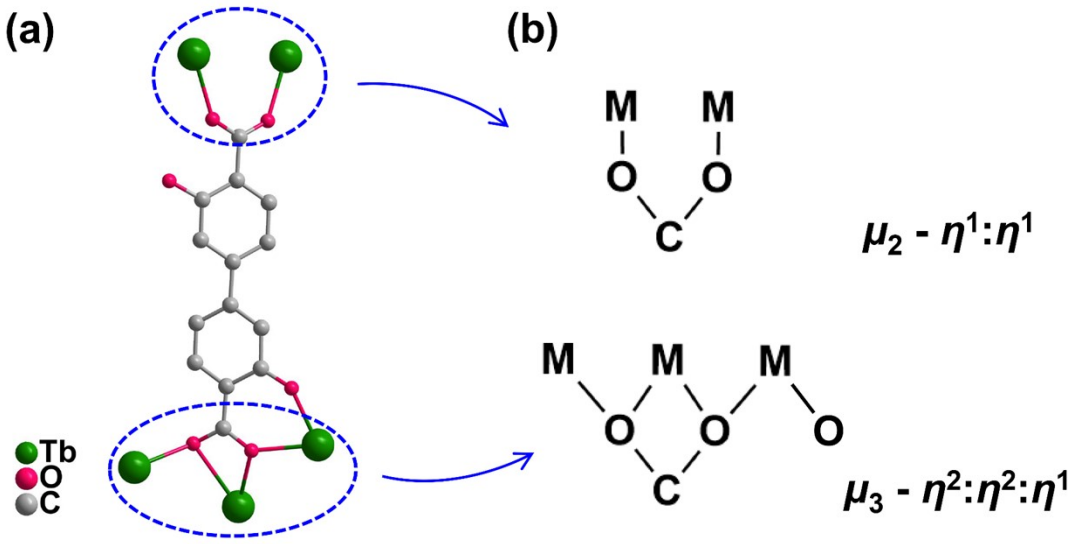

Figure S2 (a) The coordination environment of $HDOBPDC^{3-}$. (b) The coordination mode of $HDOBPDC^{3-}$.

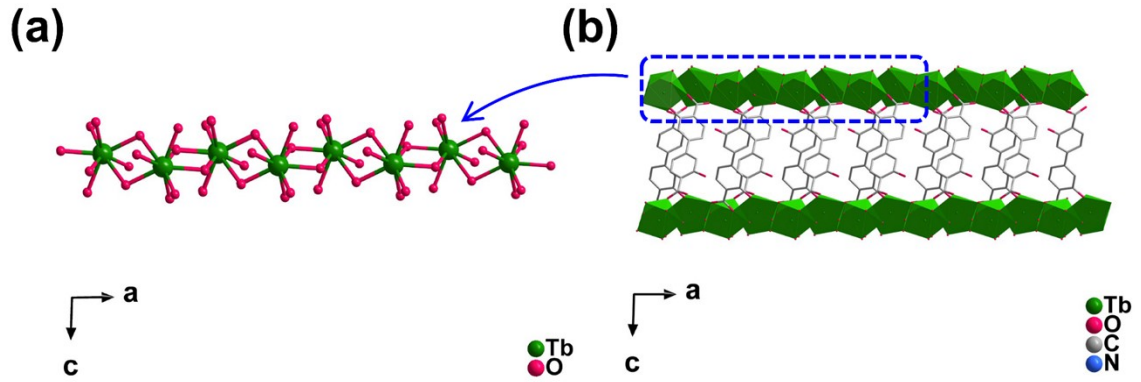

Figure S3 (a) The 1D chain structure of **Tb-MOF-1** along the *a*-axis. (b) The 2D layer of **Tb-MOF-1** aggregation along the *b*-axis. All hydrogen atoms, water molecule and DMF molecules are omitted for clarity.

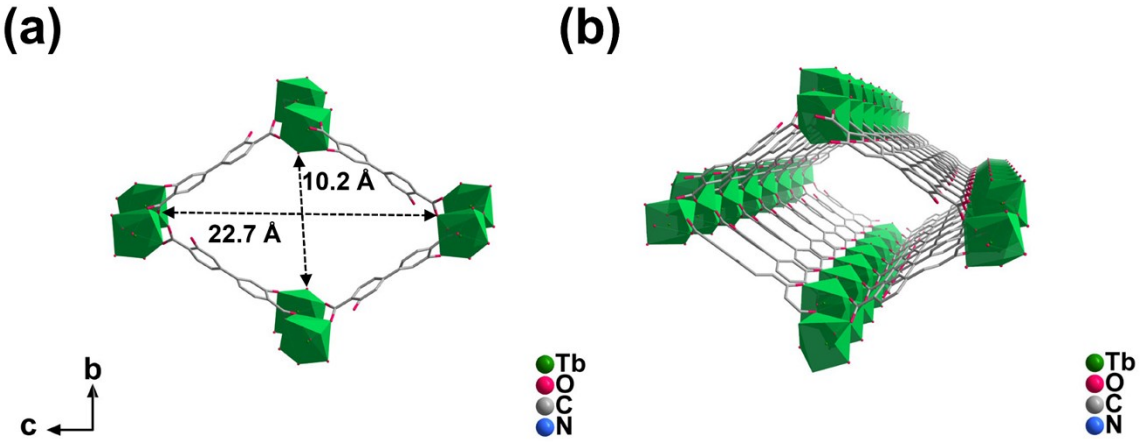

Figure S4 (a) The channel structure of Tb-**MOF-1** aggregation along the *a*-axis. (b) The 3D schematic of the channel structure in **Tb-MOF-1**. All hydrogen atoms, coordinated DMF molecules and free water molecules are omitted for clarity.

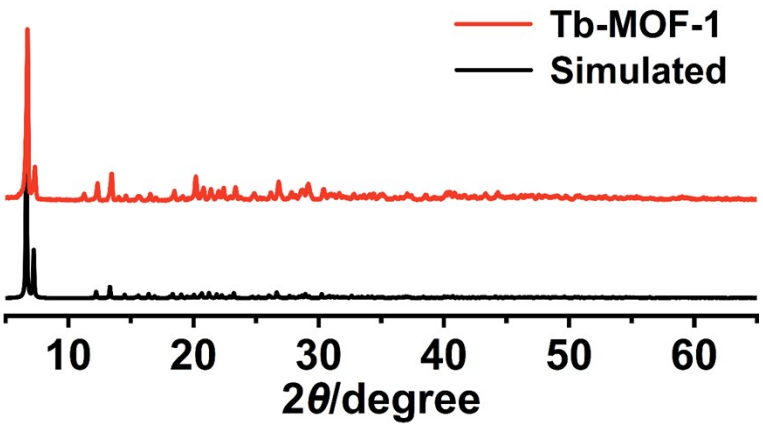

Figure S5 The powdered X-ray diffraction (PXRD) patterns of **Tb-MOF-1**.

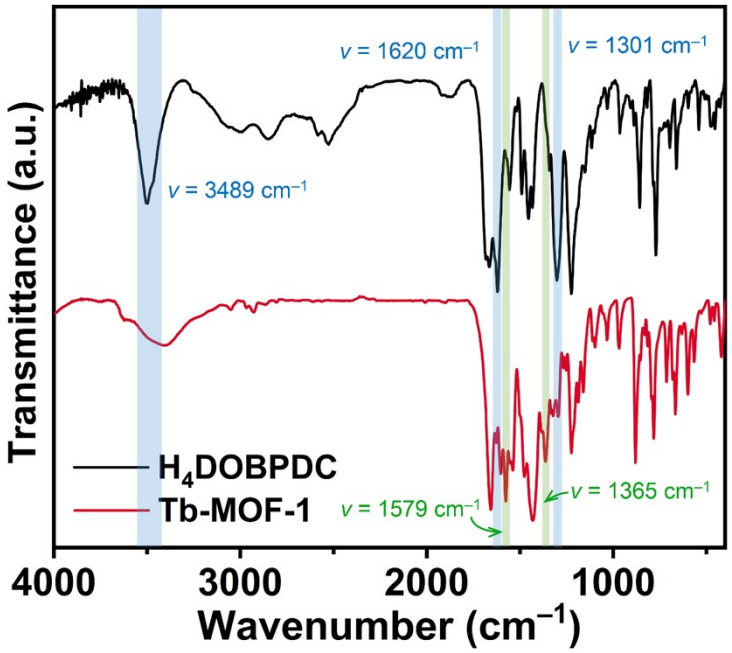

Figure S6 The FT-IR spectra of H_4DOBPDC and **Tb-MOF-1**.

Notes: Compared to the FT-IR spectra of **Tb-MOF-1**, the intensity of the C=O stretching vibration band H_4DOBPDC (ν = 1620 cm^{-1}) was substantially decreased. The O-H stretching vibrations (ν = 3489 cm^{-1}) and the bending vibration (ν = 1301 cm^{-1}) of the phenolic hydroxyl groups were both weakened.[1] Two new bands appear at the 1579 cm^{-1} and 1365 cm^{-1} in **Tb-MOF-1**, which can be assigned to the characteristic asymmetric and

symmetric stretching vibration bands of carboxylate coordination structure, respectively.[2] These IR results further confirmed the formation of coordination bonds between the Tb ions and O atoms of the carboxy and hydroxyl groups from ligand.[3]

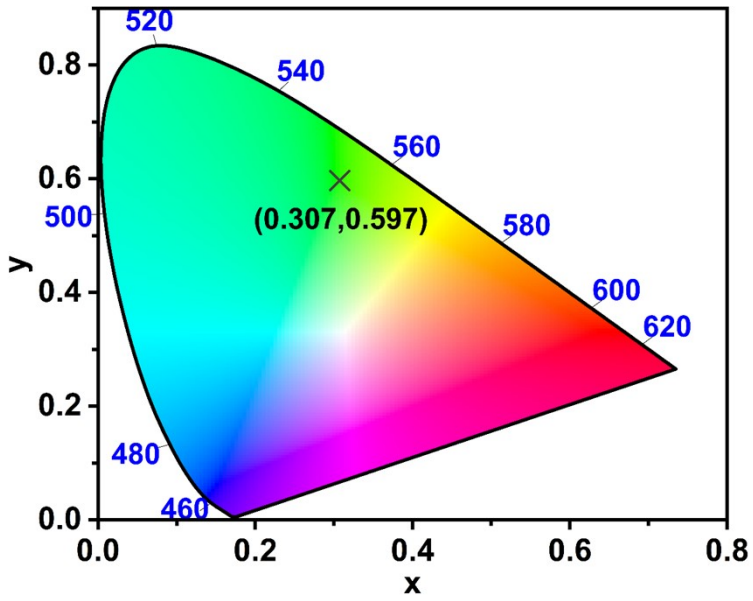

Figure S7 The photoluminescent CIE profile of **Tb-MOF-1**.

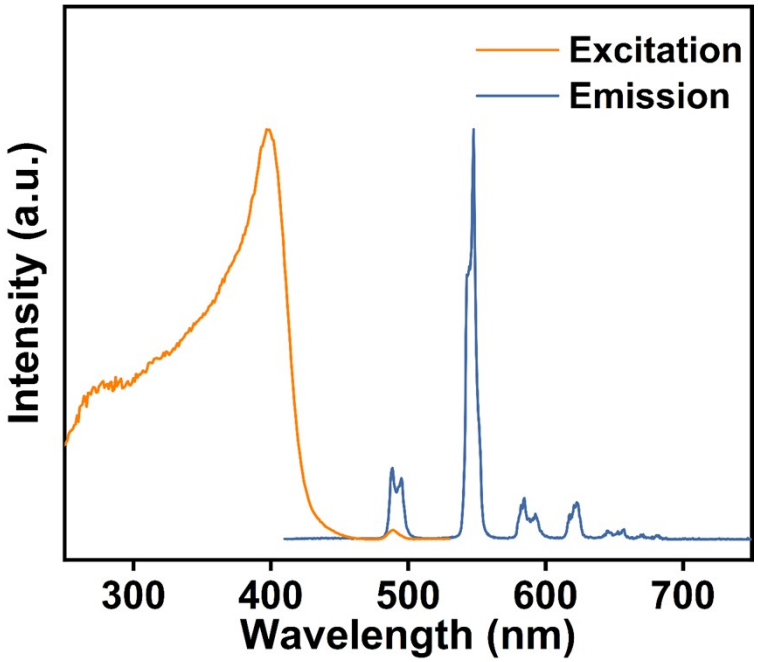

Figure S8 The solid-state PL excitation spectra and PL emission spectra of **Tb-MOF-1**.

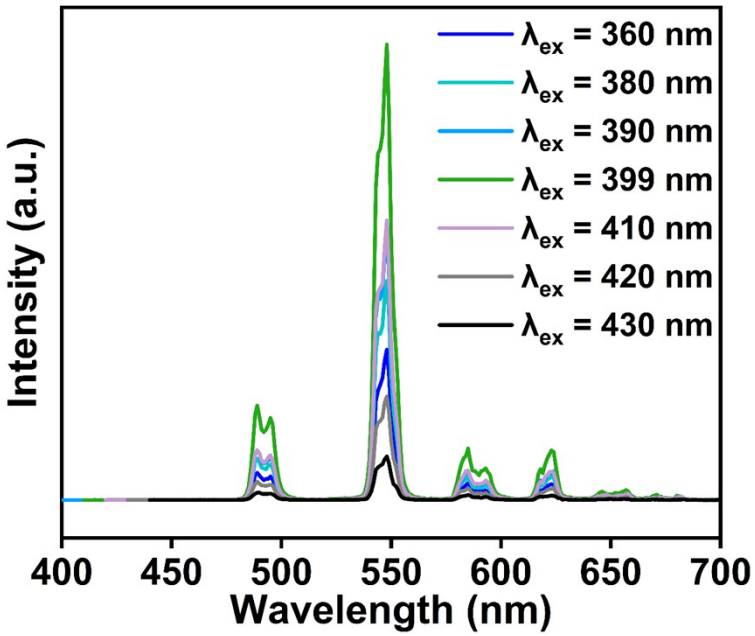

Figure S9 The solid-state PL emission spectra of **Tb-MOF-1** under different excitation wavelengths.

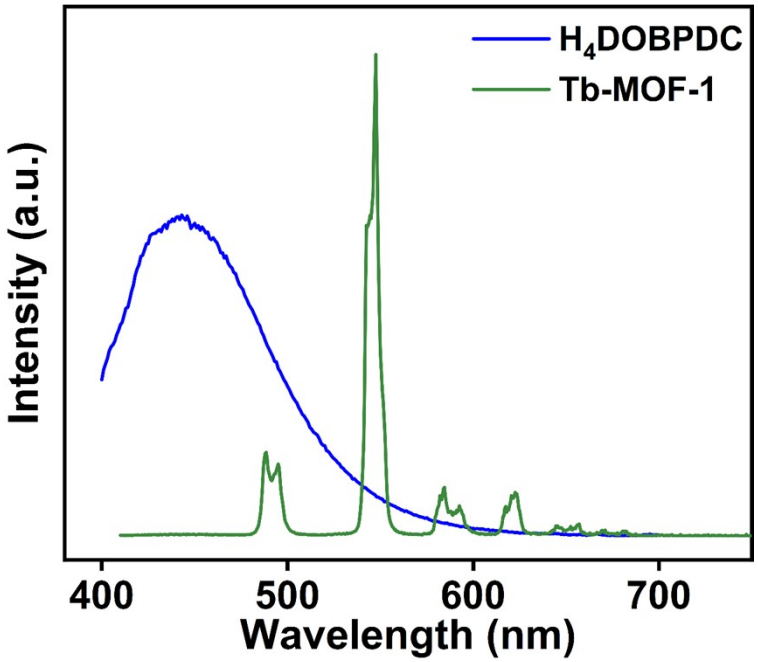

Figure S10 The solid-state PL emission spectra of ligand H_4DOBPDC and **Tb-MOF-1**.

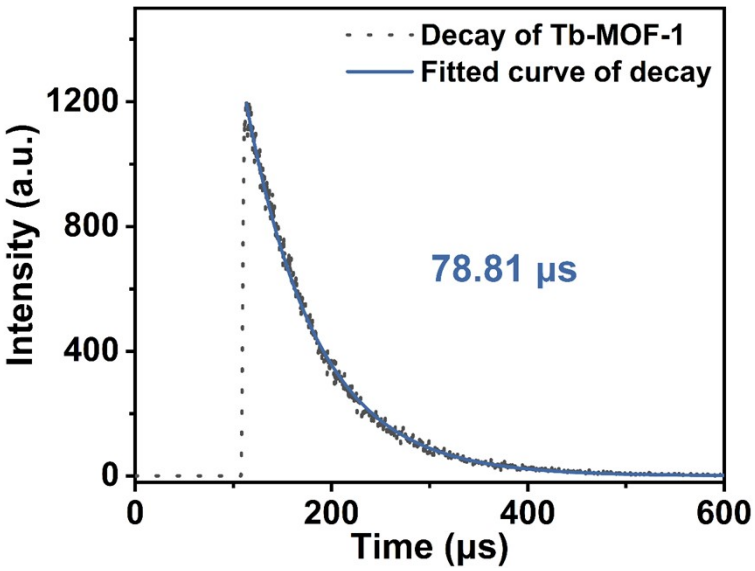

Figure S11 The PL decay time graph of solid-state **Tb-MOF-1** tested at room temperature.

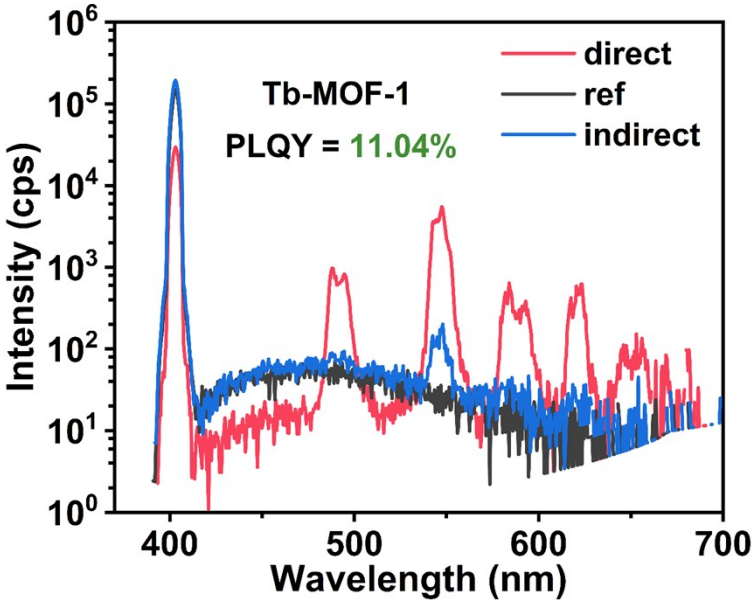

Figure S12 The PLQY spectra of **Tb-MOF-1**.

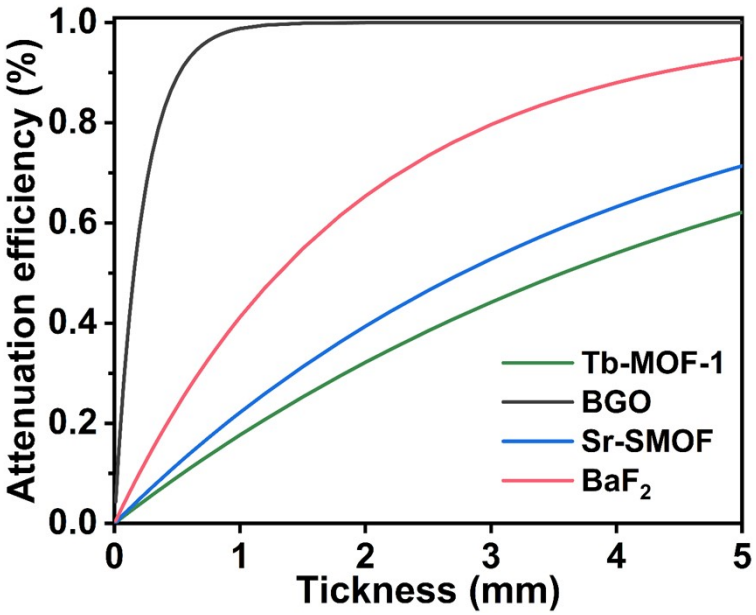

Figure S13 The X-ray attenuation efficiencies as a function of the material thickness of **Tb-MOF-1** and other references toward 50 keV X-ray photons.

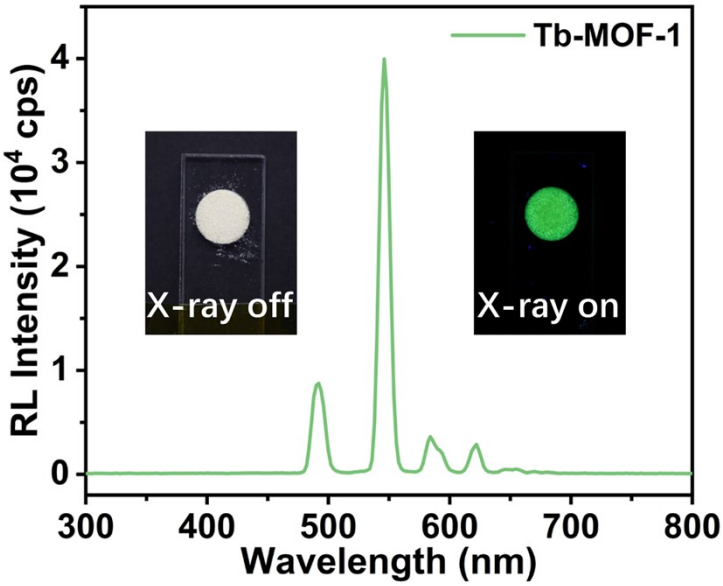

Figure S14 The RL spectra of the **Tb-MOF-1** under a dose rate of 42.29 mGy/s. The inset are the photos of **Tb-MOF-1** with X-ray off/on.

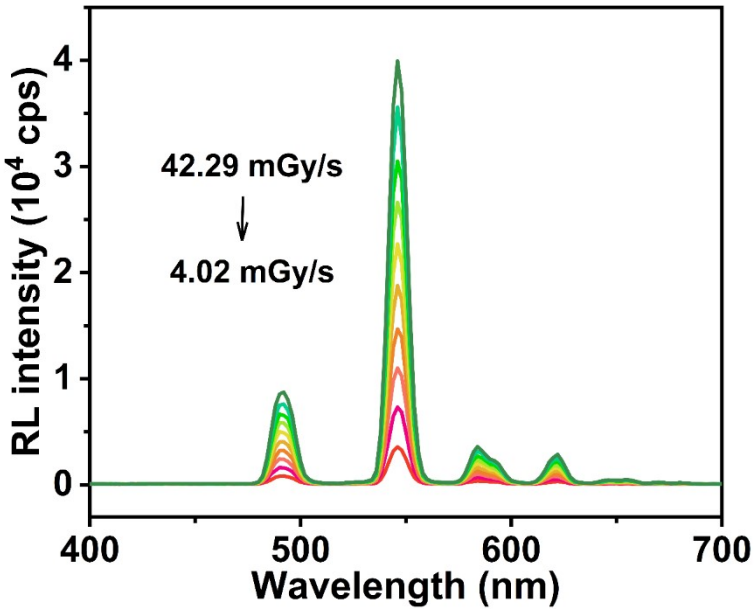

Figure S15 The X-ray dose rate dependent RL of **Tb-MOF-1** in the range from 42.29 to 4.02 mGy/s.

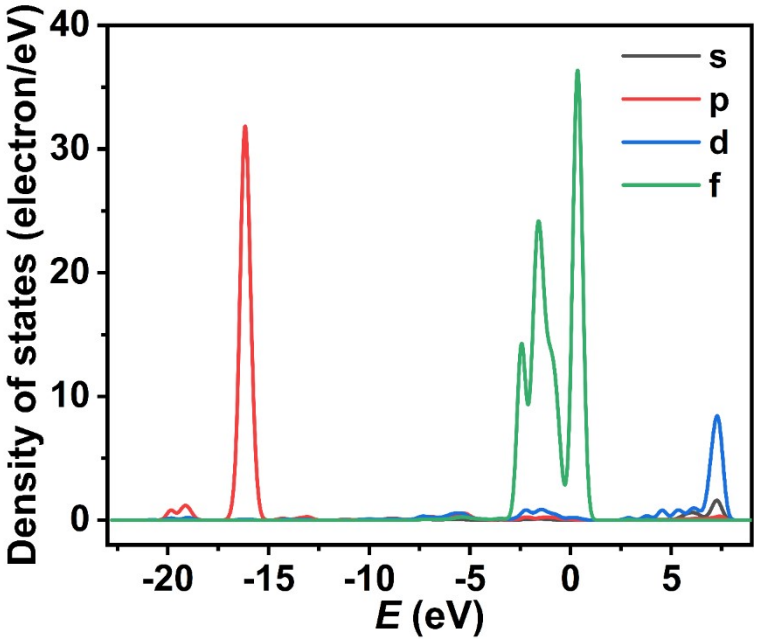

Figure S16 The partial electronic density of states of Tb^{3+} ions in **Tb-MOF-1**.

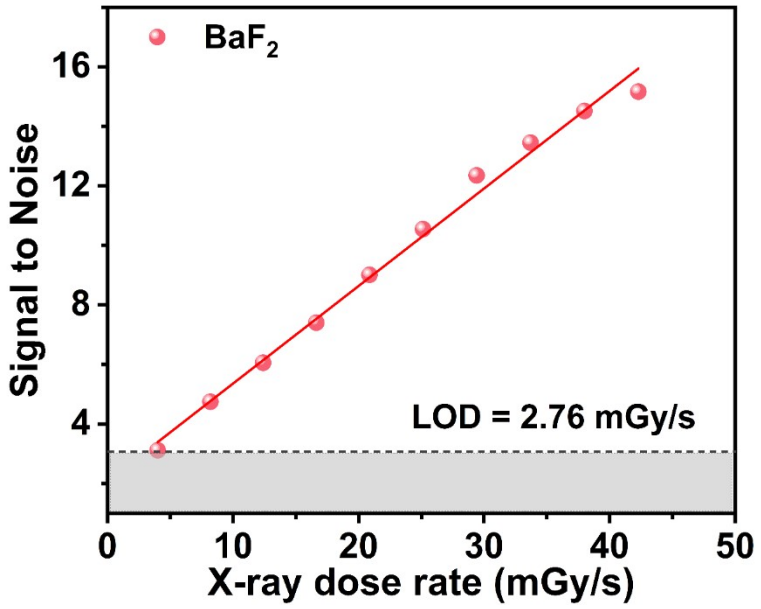

Figure S17 The detection limit of BaF_2.

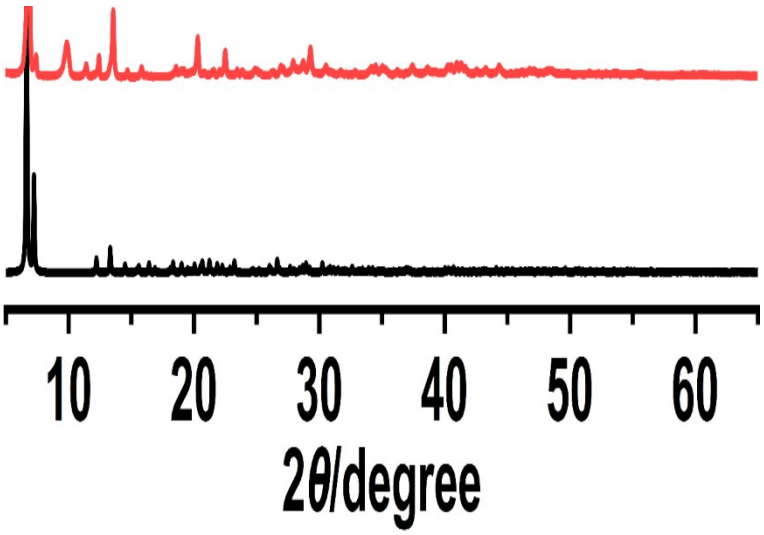

Figure S18 The PXRD result of **Tb-MOF-1** after continuous X-ray irradiation for 3 h under a dose rate of 42.29 mGy/s.

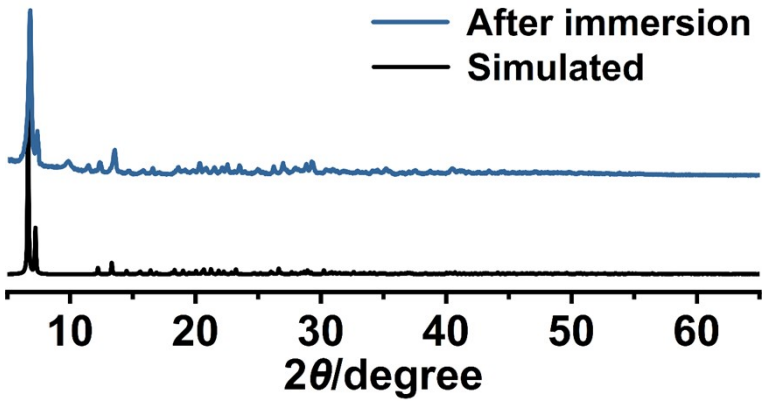

Figure S19 The PXRD result of the **Tb-MOF-1** crystals after being immersed in water for 30 d.

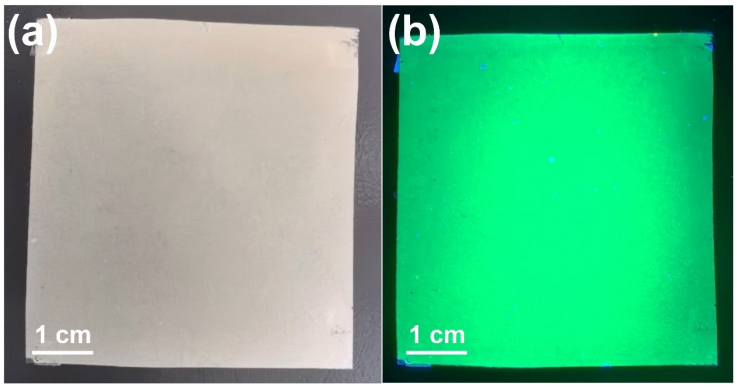

Figure S20 The photographs of the flat **Tb-MOF-screen** with UV off (a) /on (b).

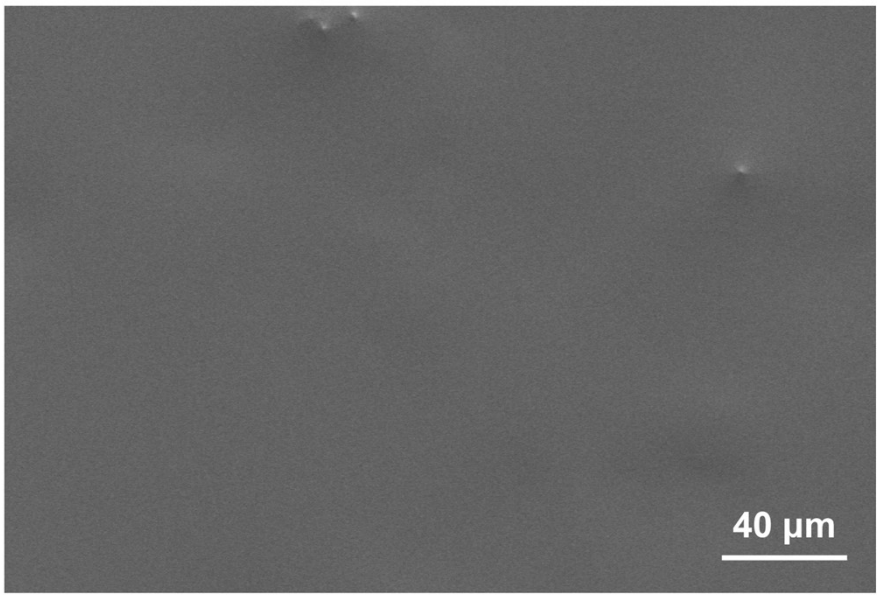

Figure S21 The SEM photo of the **Tb-MOF-screen**.

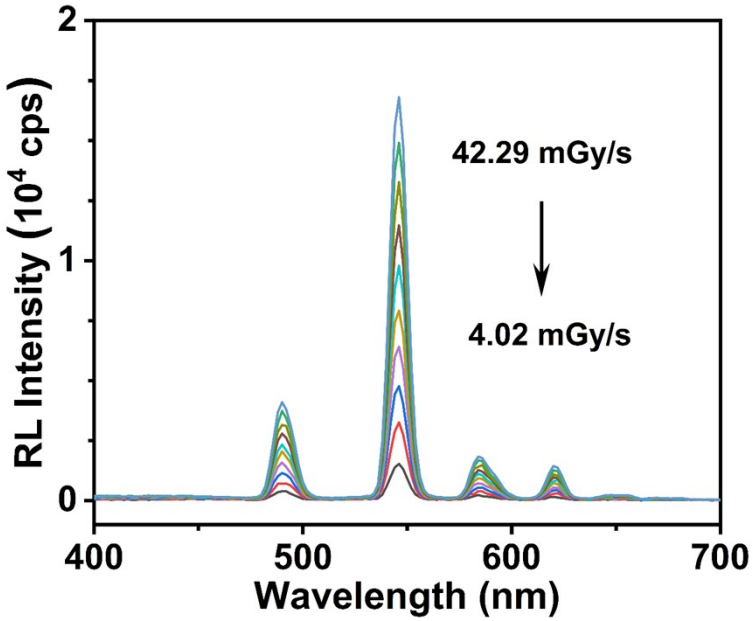

Figure S22 The X-ray dose rate dependent RL spectra of **Tb-MOF-screen** in the range of 4.02–42.29 mGy/s.

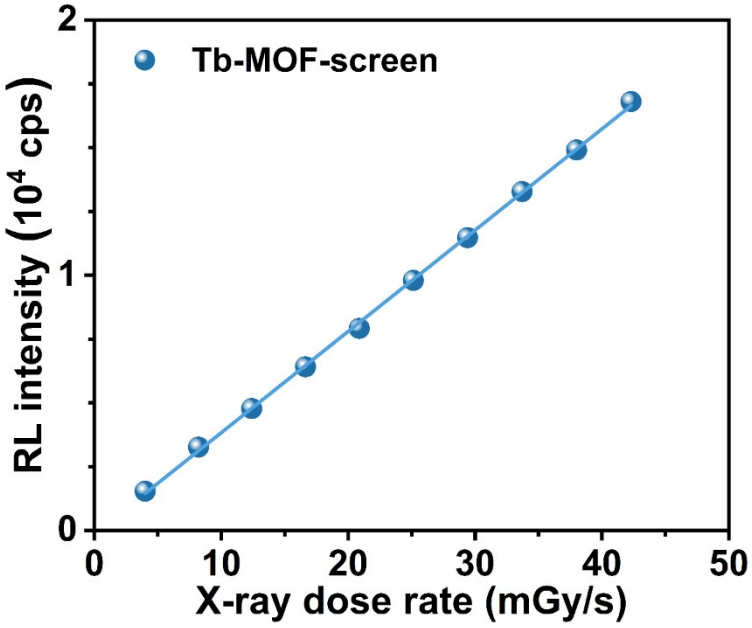

Figure S23 The linear relationship between RL intensity and X-ray dose rates of **Tb-MOF-screen**.

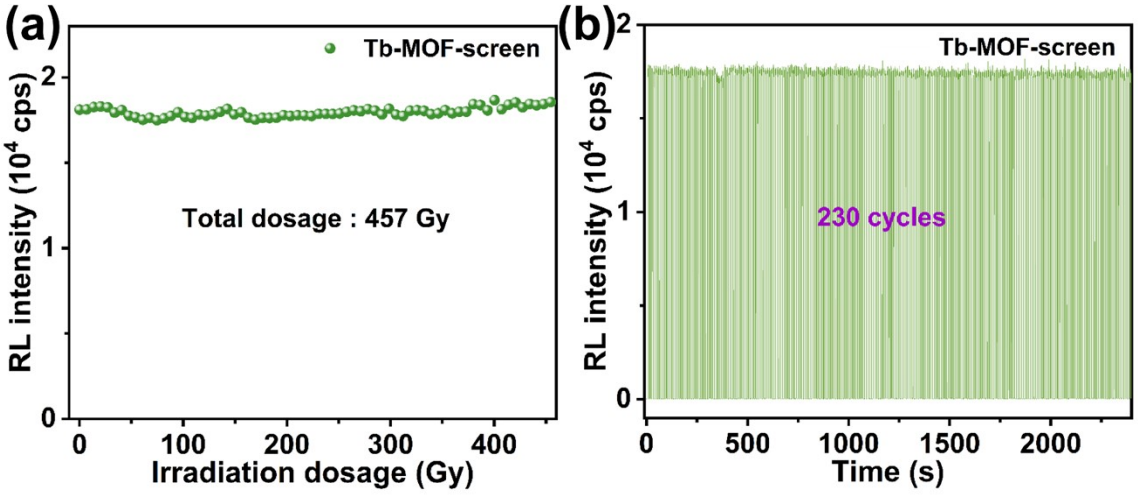

Figure S24 (a) Radiation stability of **Tb-MOF-screen** under continuous X-ray irradiation at a dose rate of 42.29 mGy/s for 3 h. (b) The RL intensities recorded for the **Tb-MOF-screen** over continuous 230 on/off cycles with the dose rate of 42.29 mGy/s.

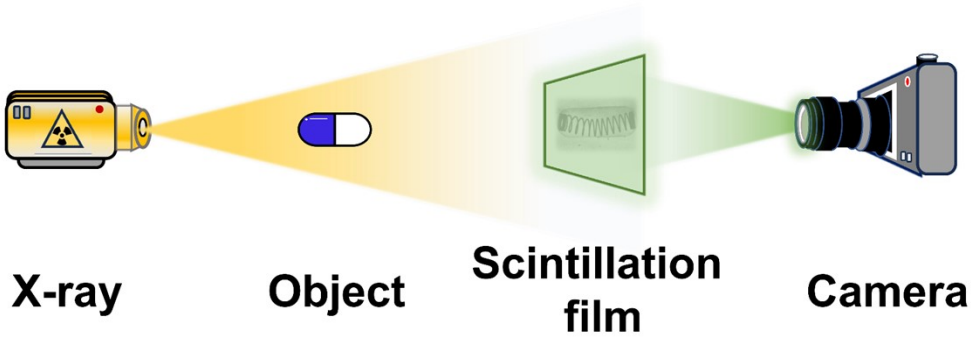

Figure S25 Schematic diagram of X-ray imaging system.

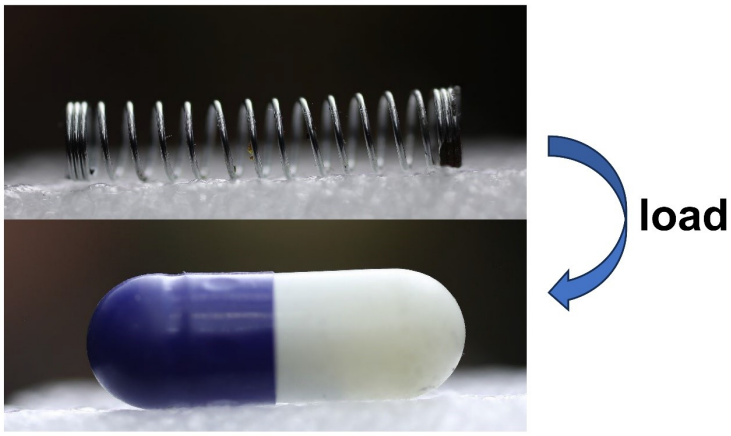

Figure S26 Schematic diagram of the spring assembled into the capsule (The physical photo of the spring(top) and individual capsule(bottom)).

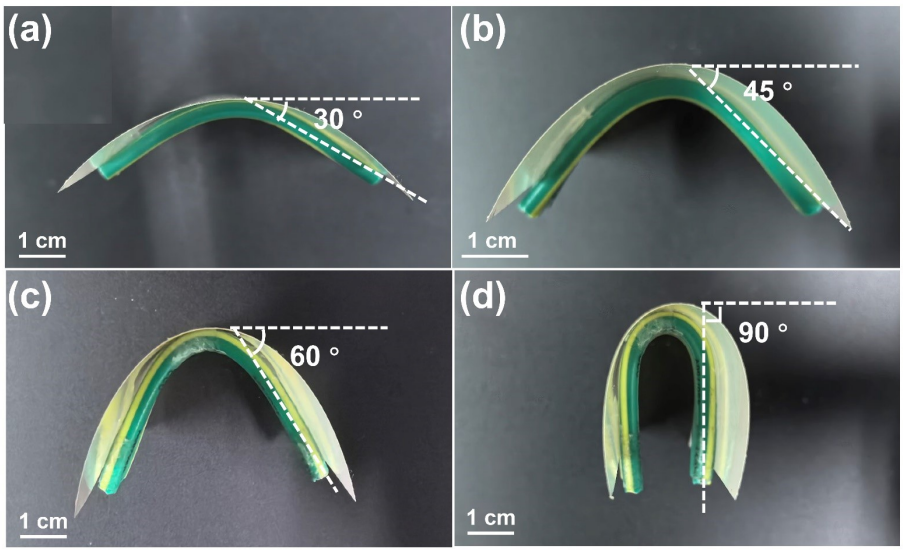

Figure S27 The photographs of the **Tb-MOF-screen** and the curved wires with different curved angles.

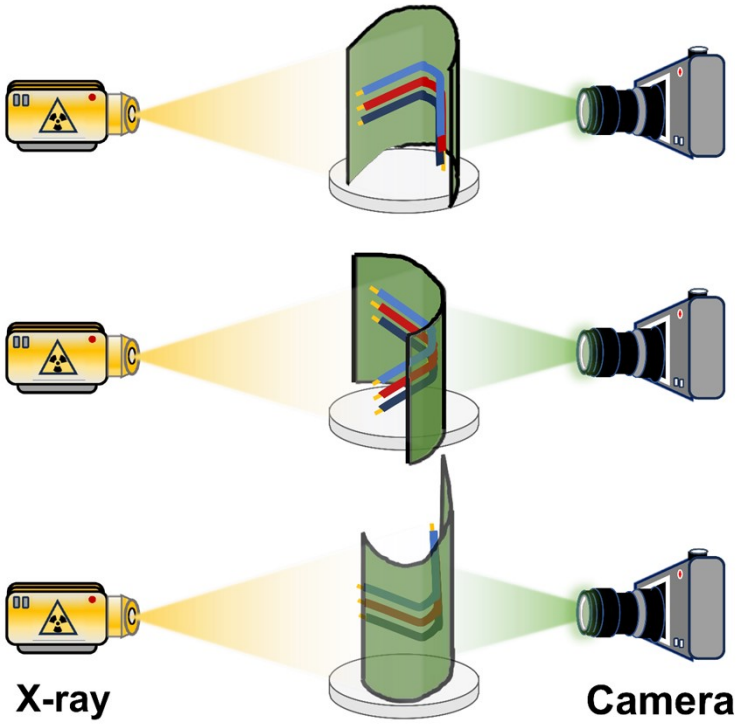

Figure S28 Schematic diagram of the different shooting angles during the X-ray imaging.

Note: The process of bending the scintillation screen and the curved wires involves initially bending the wires to a fixed angle. Subsequently, the flexible scintillation screen is secured

and tightly adhered to the wires using double-sided adhesive. The flexible scintillation screen and the bent wire are mounted on a rotatable stage, allowing the internal structure to be captured at various angles by rotating the stage.

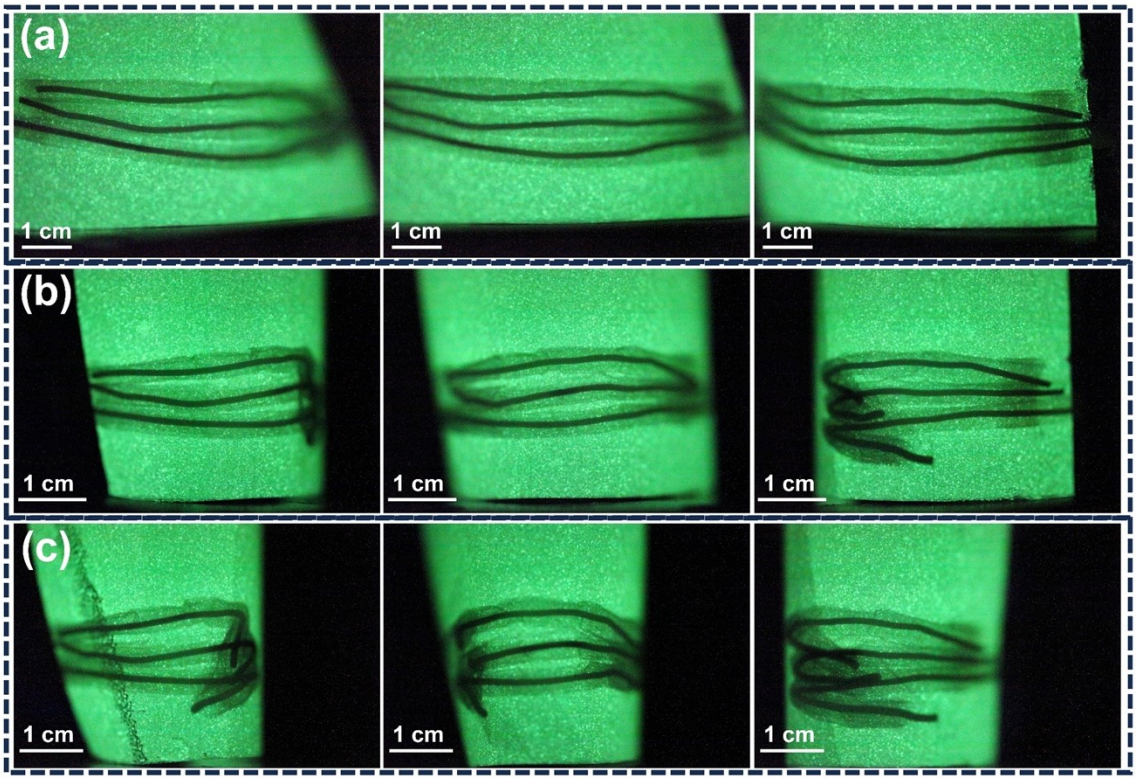

Figure S29 The X-ray imaging photos of **Tb-MOF-screen** in different directions for curved wires under different curvature radii (30°(a), 60°(b), 90°(c)).

Supplementary tables

Table S1 Crystal data and structure refinement for **Tb-MOF-1**.

	$[Tb(HDOBPDC)(DMF)(H_2O)]_n$
CCDC	2346454
Formula	$C_{17}H_{16}N_1O_8Tb_1$
M_r	521.23
Crystal system	monoclinic
Space group	$P2_1/c$
a/Å	6.3736(2)
b/Å	15.8213(5)
c/Å	24.4175(6)
α/°	90
β/°	92.222(2)
γ/°	90
V [Å^3]	2460.38(13)
Z	4
Calcd. density (g cm^{-3})	1.407
μ/mm^{-1}	2.908
F(000)	1016
2θ/°	5.632 to 50.054
Reflections collected	17403
Goodness-of-fit on F^2	1.101
Final R indices [$I > 2\sigma(I)$]	$R_1 = 0.0358$ $wR_2 = 0.1126$

[a]$R_1 = \sum(F_o - F_c)/\sum F_o$. [b]$wR_2 = [\sum w(F_o^2 - F_c^2)^2/\sum w(F_o^2)^2]^{1/2}$.

Table S2 Selected bond lengths (Å) and bond angles (°) in **Tb-MOF-1**.

Selected bond lengths (Å)			
Tb1–Tb1#1	3.8594(5)	Tb1–O4#1	2.722(4)
Tb1–O4#2	2.358(3)	Tb1–O2	2.213(4)
Tb1–O6#3	2.376(4)	Tb1–O1#1	2.407(3)
Tb1–O1	2.325(4)	Tb1–O7#4	2.358(4)
Tb1–O3	2.324(4)		
Selected bond angles (°)			
O4#1–Tb1–Tb1#2	129.47(10)	O4#2–Tb1–Tb1#2	83.09(8)
O4#1–Tb1–O4#2	73.20(13)	O4#1–Tb1–O6#3	70.48(13)
O4#1–Tb1–O1#2	102.97(13)	Tb1–O1–Tb1#2	109.29(14)
O4#1–Tb1–O7#4	138.77(13)	O2–Tb1–Tb1#2	107.10(9)
O2–Tb1–O4#1	97.62(14)	O2–Tb1–O4#2	169.45(12)
O2–Tb1–O6#3	83.89(16)	O2–Tb1–O1	72.55(13)
O2–Tb1–O1#2	139.55(13)	O2–Tb1–O7#4	110.24(15)
O2–Tb1–O3	84.42(16)	O6#3–Tb1–Tb1#2	69.28(9)
O6#3–Tb1–O4#2	97.53(13)	O6#3–Tb1–O1#2	71.08(13)
O1–Tb1–Tb1#2	36.06(8)	O1#2–Tb1–Tb1#2	34.65(8)
O1–Tb1–O4#1	145.38(13)	O1–Tb1–O4#2	117.96(11)
O1#2–Tb1–O4#2	49.77(12)	O1–Tb1–O6#3	75.43(13)
O1–Tb1–O1#2	70.71(14)	O1–Tb1–O7#4	74.05(13)
O1–Tb1–O3	133.64(15)	O7#4–Tb1–Tb1#2	70.95(10)
O7#4–Tb1–O4#2	75.28(13)	O7#4–Tb1–O6#3	140.15(13)
O7#4–Tb1–O1#2	75.05(14)	O3–Tb1–Tb1#2	148.26(10)
O3–Tb1–O4#2	88.19(15)	O3–Tb1–O4#1	75.81(15)
O3–Tb1–O6#3	142.34(14)	O3–Tb1–O1#2	134.19(15)
O3–Tb1–O7#4	77.33(14)	Tb1#5–O4–Tb1#2	106.80(13)

Symmetry codes: #1 1 + *x*, *y*, *z*; #2 1 – *x*, –*y*, 1 – *z*; #3 1 – *x*, –1/2 + *y*, 1/2 – *z*; #4 *x*, 1/2 – *y*, 1/2 + *z*; #5 –1 + *x*, *y*, *z*.

Table S3 Comparison of the performances for some commercially used scintillators.

Compound	Detection limit (μGy/s)	Decay time (μs)	Spatial resolution (lp/mm)	Reference
Tb-MOF-1	1.71	78.81	7.7	This work
CsI:Tl	0.116	0.608	5.0	[4]
Gd_2O_2S:Tb	NA	621.87	3.0-6.0	[4, 5]
BaF_2	＞5.5	0.0006	NA	[6]

NA: Not available

Supplementary references

[1] Y. Ou, W. Zhou, Z. Zhu, F. Ma, R. Zhou, F. Su, L. Zheng, L. Ma and H. Liang, Host Differential Sensitization toward Color/Lifetime-Tuned Lanthanide Coordination Polymers for Optical Multiplexing, *Angew. Chem. Int. Ed.*, 2020, **59**, 23810–23816.

[2] W. Xu, N. Hanikel, K. A. Lomachenko, C. Atzori, A. Lund, H. Lyu, Z. Zhou, C. A. Angell and O. M. Yaghi, High-Porosity Metal-Organic Framework Glasses, *Angew. Chem. Int. Ed.*, 2023, **62**, e202300003.

[3] Z. Su, Y.-R. Miao, G. Zhang, J. T. Miller and K. S. Suslick, Bond Breakage under Pressure in a Metal Organic Framework, *Chem. Sci.*, 2017, **8**, 8004–8011.

[4] X.-Y. Du, S. Zhao, L. Wang, H.-D. Wu, F. Ye, K.-H. Xue, S.-Q. Peng, J.-L. Xia, Z.-R. Sang, D.-D. Zhang, Z.-P. Xiong, Z.-P. Zheng, L. Xu, G.-D. Niu, J. Tang, Efficient and ultrafast organic scintillators by hot exciton manipulation, *Nat. Photonics,* 2024, **18**, 162-169.

[5] H.-R. Zou, W.-J. Zhu, J.-T. Zhao, S. Zhou, S.-Q. Xu, and L. Lei, Sub-10 nm Lanthanide-Doped $Lu_6O_5F_8$ Nanoscintillators for Real-Time High-Resolution Dynamic 3D X-Ray Imaging, *Adv. Funct. Mater.* 2024, 2409156.

[6] T. Yanagida, T. Kato, D. Nakauchi and N. Kawaguchi, Fundamental aspects, recent progress and future prospects of inorganic scintillators, *Jpn. J. Appl. Phys.*, 2023, **62**, 010508.